Direct Saturation MRI: Theory and Application to Imaging Brain Iron

S. A. Smith[1,2], J. W. Bulte[2,3], and P. C. van Zijl[1,2]

[1]F.M. Kirby Center, Kennedy Krieger Institute, Baltimore, MD, United States, [2]Russell H. Morgan Department of Radiology, Johns Hopkins University, Baltimore, MD, United States, [3]Chemical and Biomolecular Engineering, Johns Hopkins University, Baltimore, MD, United States

Introduction: Iron is one of the most important endogenous metals in the human body and is linked to devastating diseases such as Alzheimer's. Current iron studies employ T_2/T_2*w imaging. Interestingly, 3T magnetization transfer (MT) imaging recently showed a significant MTR difference between cerebral gray matter (GM) regions (1) known to differ in iron content (2). Zurkiya and Hu (3) demonstrated that off-resonance RF saturation effects were proportional to iron content and others suggested that tissue iron affects the magnetization transfer ratio (MTR) in cerebral GM (4). We hypothesized that the link between GM MTR and iron is due to direct water saturation (DS): affected by iron through a T_2 decrease that broadens the saturation lineshape (5). Measurement of the direct water saturation lineshape should reflect this in the brain. Direct saturation can be accomplished by minimizing contributions of MT effects and can be simulated using the Bloch equations (5). Analogously to the MTR we write the direct saturation ratio: DSR = $1-S(\omega)/S_o$, where $S(\omega)$,S_o are the signals with and without RF irradiation. After optimization, we found that DSR imaging highlighted all cerebral GM structures and that the DSR signals in these regions were directly proportional to iron content. Excellent agreement was found between the predicted and the experimentally measured DSR. We also examine the T_1 contribution to saturation in detail.

Methods: Simulation: The effect of power on the saturation spectrum was examined by comparing $1-S(\omega)/S_o$ from the Bloch equations with and without MT (6) as a function of frequency with an input of 3T GM relaxation times (T_2=70ms,T_1=1.1s). The power suitable for DS (i.e. sufficiently selective, largely devoid of MT) was determined and used in the exact Bloch equations (5) to probe the offset frequency most sensitive to a 15% T_2 change. ***In Vivo*:** Five healthy adults (22-40yr) were scanned after written, informed consent. All experiments were performed on a 3.0T MRI scanner using body coil excitation and SENSE head coil for reception. The effects of susceptibility differences were minimized by applying 2nd order shimming over the entire volume. Absolute R_2=1/T_2 (double-echo SE: TR/TE_1/TE_2 = 2500/30/80ms, nom. resolution 1.2x1.2x2.2mm) and T_2*-weighted (multi-slice GRE, TR/TE/α = 575ms/ 30ms/20°, nom. resolution 1.2x1.2x2.2mm^3) were acquired. DSR experiments: axial volumes from the basal ganglia to brainstem (10 slices), multi-slice, multi-shot EPI (factor x 9) GRE (TR/TE/α = 3s/5.8ms/90°), nom. resolution 1.8x1.8x3mm. RF: 250ms block pulse (0.8 μT), 27 offset frequencies (with respect to water, -750 - 750 Hz), plus a reference scan (no irradiation). DSR was calculated voxel-by-voxel. Susceptibility differences introduce shifts of the water frequency in each voxel and were corrected by centering the DSR spectrum to 0 Hz: the acquired DSR spectrum was interpolated and fitted to a polynomial; the offset where the polynomial was maximal was assigned to 0 Hz and the DSR spectrum at each voxel was shifted accordingly. From the corrected DSR images, ROIs were manually selected in the globus pallidus (GP), putamen (Put), caudate nucleus (CN), thalamus (Thal), periventricular white matter (WM), red nucleus (RN), substantia nigra (SN), and cortex (crtx). These regions were also selected on the T_2*w and R_2 images. The DSR signal in each ROI was compared to age-adjusted iron concentration (2).

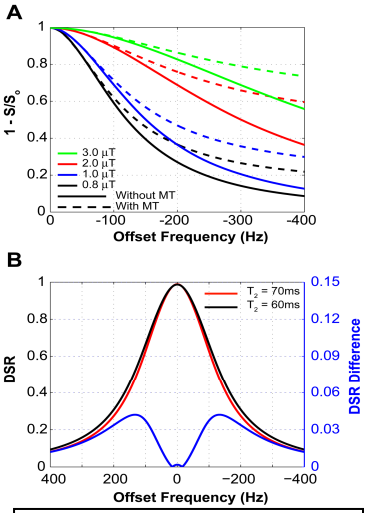

Figure 1: A) Simulation of RF saturation with and without MT as a function of pulse amplitude, B) analytical solution showing max. difference in DSR (blue)

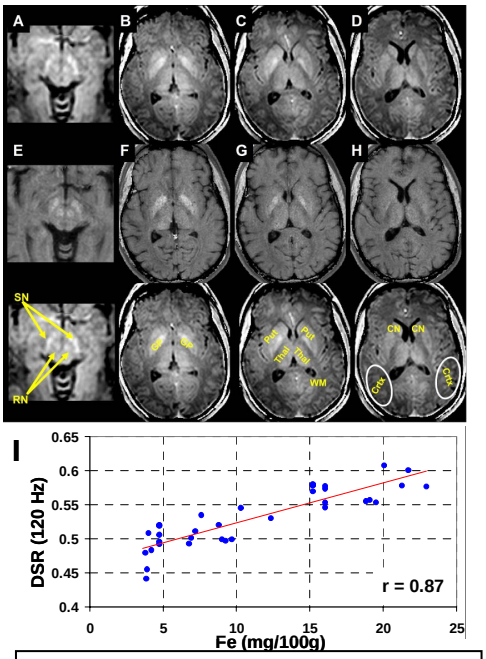

Figure 2: A – D) DSR (120 Hz), E-H) R_2 maps, I) plot of DSR (120 Hz against age-adjusted Iron concentration with regression line (red)

Results and Discussion: Fig 1A: power effect on saturation spectra with (dash) and without (solid) MT. MT effects dominate at higher power and offset frequencies. We therefore chose B_1 = 0.8μT for *in vivo*. **Fig 1B:** raw (red, black) and difference DSR spectra (blue) which peaks at (120-140Hz); 120 Hz was chosen for *in vivo*. **Fig 2:** DSR (120 Hz) and R_2 maps of the brainstem (**A,E,** respectively) and basal ganglia (**B-D**, **F-H**, respectively). High contrast between GM structures rich in iron (RN,SN,GP) and surrounding tissue are appreciated in DSR and R_2 images. However, in structures containing less iron (Put, Thal, Crtx, CN), DSR images still show excellent contrast (**Fig 2 B-D**), while R_2 appears somewhat bland (**Fig 2F-H**). **Fig 2I** reveals the DSR (120 Hz) is significantly related to iron (r=0.87,p= 0.001). Differences in GM MTR can be explained by direct saturation effects that are proportional to the tissue iron content. But, is the relationship between DSR and iron solely T2-driven or a combination of T_1 and T_2? Except for the GP,SN,RN, the basal ganglia GM regions (**Fig. 2F-H**) are not well seen in the R_2 images, neither is the distinction between WM and GM. Therefore DSR contrast in other GM areas needs to be explained by T_1, which has been reported to depend on iron and water content (7). GM T_1 is much longer than that of white matter, making all GM visible on DSR images. The influence of an iron-based T_1-effect on the DSR should oppose T_2 (i.e. reduction of the DSR) because T_1 decreases with increasing iron (7). However this decrease has been shown to be primarily due to a tissue water density decrease. Thus, the effect of paramagnetic agents on T_2 is larger than their effect on T_1, and ultimately dominates the iron-dependency in the DSR spectrum. Interestingly, the DSR sequence can perhaps serve as an alternative method to measure T_1 without MT and inter-compartmental exchange effects. We calculated T_1 from DSR and T_2 measurements, using the analytical Bloch equations. The resulting values in Table 1 reveal that the calculated GM T_1 values are all within ~ 100ms (smaller spread than in the literature (6)). Furthermore, correlations of water density and estimated T_1 with iron content were not significant (Fe:T_1, r=0.21, p=0.61, Fe:water density, r=0.23, p=0.57). However, the water content, T_1 correlation persisted (r=0.81, p=0.02). Thus the present calculation removes the artificial dependency of T_1 on iron content.

Structure	FE (mg/100g)*	fw	T2 (ms)	DSR	T1 Estimate (ms)	T1 (ms)†
GP	21.3 ± 3.5	0.73	53.6 ± 4.5	0.570 ± 0.023	882	1043 ± 37
RN	19.5 ± 6.9		59.0 ± 4.8	0.565 ± 0.015	932	
SN	18.5 ± 6.5	0.76	52.7 ± 4.7	0.581 ± 0.011	904	1147 ± 50
Put	13.3 ± 3.4	0.79	71.7 ± 3.7	0.514 ± 0.22	927	1337 ± 42
CN	9.28 ± 2.1	0.82	76.6 ± 5.6	0.511 ± 0.016	990	1483 ± 42
Thal	4.8 ± 1.2	0.73	68.9 ± 3.7	0.506 ± 0.013	890	1218 ± 40
Crtx	3.8 ± 0.7	0.86	88.6 ± 7.6	0.473± 0.026	975	1763 ± 60
WM	4.2 ± 0.9	0.71	75.2 ± 4.9	0.434 ± 0.003	704	847 ± 43

Conclusion: Direct saturation imaging was performed in human brain and clearly discriminated GM regions, which resulted from the DSR dependence on both T_2 shortening and a longer T_1 compared to WM. Further applications in populations with iron-related diseases will shed light on the sensitivity/specificity of this approach. Combining DSR with T_2 imaging, revealed a novel opportunity to determine T_1 independent of iron content and less dependent on exchange. These first direct saturation measurements *in vivo* are thus providing a new opportunity to study tissue properties. **References: 1)** Smith SA, et al. MRM 2006;56:866-875. **2)** Hallgren B, Sourander P.J. Neurochemistry 1958;3:41-51. **3)**Zurkiya O, et al. MRM 2006;56:726-732. **4)** Elster AD, et al. Rad 1994;190:541-546. **5)** Mulkern RV, Williams ML. Med Phys 1993;20:5-13. **6)** Stanisz GJ, et al. MRM 2005; 54:507-512. **7)** Gelman N, et al. MRM 2001;45:71-79. **Grant Acknowledgement**: NIH/NCRR (P41 RR015241).